

Variation of Initial Bulk Residual Stresses in Aluminum Alloy 7050-T7451 and Its Effect on Distortion of Thin-Walled Structural Parts



Daniel Weber, Benjamin Kirsch, Nicholas A. Bachus, Christopher R. D'Elia, Barbara S. Linke, Michael R. Hill, and Jan C. Aurich

Abstract Milled thin-walled monolithic aluminum structural parts are widely used in the aerospace industry due to their appropriate properties such as a high overall strength-to-weight ratio. The semifinished products made of aluminum alloy 7050 undergo a heat treatment to gain this increased strength and hardness: Typically, three steps including solution heat treatment, quenching, and age hardening are carried out. This also leads to high initial bulk residual stresses (IBRS) within the part in the range of ± 200 MPa. In rolled aluminum plate, plastic stretch (T7451 heat treatment designation) provides very effective relief of residual stress, decreasing IBRS to a level of ± 20 MPa. In large parts with low bending stiffness, even that low level of IBRS can cause appreciable distortion. Besides the IBRS, the machining-induced residual stresses (MIRS) contribute to the distortion. This study investigates how IBRS in different stress relieved 7050-T7451 semifinished products vary and how this variation affects the distortion of milled thin-walled monolithic structural parts. A linear elastic finite element distortion prediction model, which considers the IBRS as well as the MIRS as input, was used to analyze the effect of varying IBRS on the distortion for different part sizes and geometries. The model was validated by machining of those parts and measuring their distortion. IBRS were measured via slitting technique and MIRS via incremental hole-drilling.

Keywords Residual stress · Distortion · Milling · Aluminum 7050-T7451 · Finite element modelling

Introduction

Aluminum alloys appear as structural materials in various industries such as aerospace, automotive, electrical, and chemical [1]. For example, the aerospace industry demands a high mass fraction of aluminum alloys in airplanes. Especially thin-walled, monolithic structural components are used due to their beneficial properties, such as a high overall strength-to-weight ratio and good fatigue life [2]. Typically, those structural components are machined by the manufacturing process milling, removing up to 95% of the total volume of the semifinished product [3]. Part distortion is a common problem due to the required small wall thicknesses of those weight-optimized structural components [4]. Residual stresses (RS) in the form of machining-induced residual stresses (MIRS) and initial bulk residual stresses (IBRS) are known to be the main cause of those distortions [4]. The MIRS are induced by the machining process due to plastic deformations in a near surface layer of the part. Prior research has investigated the effects of cutting conditions and tool properties on MIRS [5–8]. The IBRS are present in the blank material because of upstream processes like rolling, casting, and especially the heat treatment, which is characterized for wrought and cast aluminum alloys by a three-step process to increase the material strength and hardness: solution heat treatment, quenching, and age hardening [9]. Especially the high thermal gradients during quenching lead to high IBRS in the range of -150 to $+100$ MPa within the material. Therefore, a RS relief through controlled stretching or compression is necessary. Although the RS can be reduced to a level of ± 20 MPa or lower, distortion remains as a problem. Past investigations showed that the position of the finished part in the semifinished product has an influence on the part distortion due to the redistribution of the IBRS [10–14]. However, it was not investigated yet how IBRS in different batches of A7050-T7451 vary and if that affects the distortion of thin-walled structural parts.

D. Weber (✉) · B. Kirsch · J. C. Aurich

Institute for Manufacturing Technology and Production Systems, RPTU in Kaiserslautern, Kaiserslautern, Germany
e-mail: daniel.weber@rptu.de

N. A. Bachus · C. R. D'Elia · B. S. Linke · M. R. Hill

Department of Mechanical and Aerospace Engineering, University of California, Davis, CA, USA

© The Society for Experimental Mechanics, Inc. 2024

C. Franck et al. (eds.), *Challenges in Mechanics of Biological Systems and Materials, Thermomechanics and Infrared Imaging, Time Dependent Materials and Residual Stress, Volume 2*, Conference Proceedings of the Society for Experimental Mechanics Series, https://doi.org/10.1007/978-3-031-50470-9_5

Numerical simulation models, typically based on the finite element method (FEM), are the preferred choice for predicting the part distortion due to known RS, because of the reduced effort of the modelling process especially for complex part geometries in comparison to analytical methods. The RS used as input for the FEM distortion model are either measured [14–16] or predicted analytically or numerically [2]. The FEM distortion models are mostly based on linear material elasticity. The modelling of the material removal process, e.g., realized by element deletion techniques [15, 16] or the application of the RS to the final machined part geometry [2, 14], was presented in the literature. Either way, forces and moments act as a consequence of the RS imbalance, which leads to the distortion of the part due to the re-equilibrium of the RS as soon as the component is released from its constraints (clamping).

In our past research, we investigated the effect of varying MIRS on distortion [17]. Furthermore, we developed a FEM model to predict the part distortion due to both MIRS and IBRS [18–20]. This study investigates how the IBRS in different 7050-T7451 semifinished products vary. With the help of the FEM distortion model, we assess how this variation affects distortion of structural parts.

Methods

Prior to investigating the effect of IBRS on distortion, the IBRS in three different configurations of material A7050-T7451 were measured by the slitting method. Then, machining of different part geometries and measuring their distortion was done to validate predictions from the FEM distortion model.

Initial Bulk Residual Stress Measurements

To investigate the effect of IBRS on distortion, IBRS in three different A7050-T7451 materials were determined:

- A: Vendor I (USA; 102-mm-thick plate): $206 \times 28 \times 102 \text{ mm}^3$ (x -direction is longitudinal (L), rolling direction; y -direction is long-transverse (LT) direction; z -direction is short transverse (ST) direction)
- B: Vendor II (Ger; 30-mm-thick plate) batch i: $206 \times 102 \times 30 \text{ mm}^3$ (x - is L direction; y - is LT direction; z - is ST direction)
- C: Vendor II (Ger; 30-mm-thick plate) batch ii: $206 \times 102 \times 30 \text{ mm}^3$ (x - is L direction; y - is ST direction; z - is LT direction)

For two material batches, B and C, small beam specimens (see Fig. 1a), measuring $100 \times 5 \times 30 \text{ mm}^3$, were cut from the original larger stock. For each material batch, one beam specimen had its length along the rolling (L) direction and the other along the long transverse (LT). The IBRS component acting along the length of each beam specimen was measured using the slitting method, which comprises cutting the sample by wire EDM as shown in Fig. 1a (lower portion) in increments of cut depth, measuring strain after each cut depth and computing residual stress from the strain versus cut depth data [21]. Slitting provides a profile of the stress component perpendicular to the slitting plane (i.e., along the beam length in these experiments) as a function of distance along the slitting direction; the stress so determined reflects an average through the part depth (here along the 5 mm dimension of the beam). Strains were measured using metallic foil gages with active length 1.57 mm that were mounted on the back face of the beam specimens, opposite the start of the cut (see Fig. 1). Strains were measured after each of 40 equal cut depth increments, the final cut depth being equal to 95% of the 30 mm beam width. Residual stresses were computed using pulse regularization, as described earlier [21]. The residual stress measurement procedure for batch A was quite similar but for a larger plate thickness. The procedure and measurement results are presented in [22]. Measured IBRS are compared with literature values from Prime and Hill [21] (see section “Results”) and used as an input for the FEM distortion model (see section “FEM Distortion Model”).

Distortion Experiments

To validate the FEM distortion model, different samples, varying in their part geometry, IBRS, and milling path strategy, were manufactured. Besides, the position of the final part within the original block, here called “z-offset,” was also varied. Two part geometries, varying in size and complexity, were machined: a simple small rib-typed structural part with two pocket

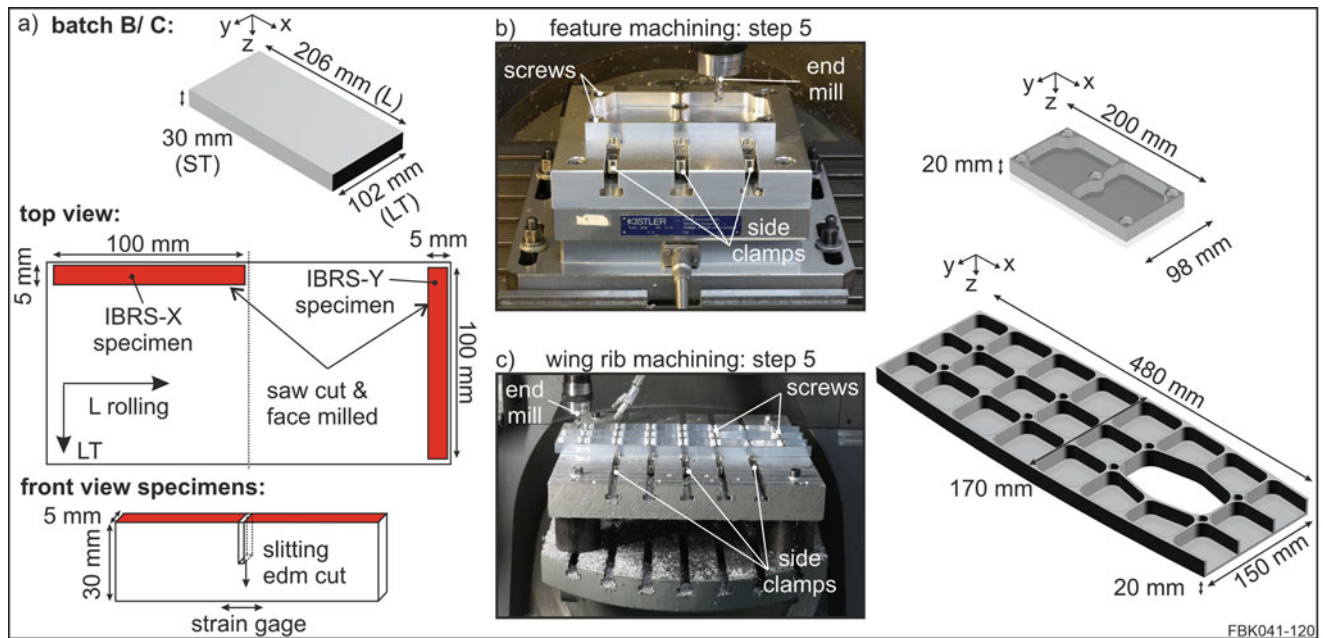


Fig. 1 Orientation of samples with slitting measurement plan (a) and experimental setups for machining of feature samples (b) and wing ribs (c)

features and one stiffener in the center (here called “feature sample,” dimension $200 \times 98 \times 20 \text{ mm}^3$; see Fig. 1b) and a more complex and bigger geometry imitating a small-scaled airplane wing rib with multiple pockets and stiffeners (here called “wing rib,” dimension $480 \times 170 \times 20 \text{ mm}^3$; see Fig. 1c) were analyzed. The feature sample was machined out of material batch B, originating from the same raw material, whereas the wing rib corresponds to material batch C. All components were machined on a five-axis DMG Mori DMU 70 CNC¹ machine. The manufacturing steps of the feature sample can be found in the literature [19]. The machining of the wing rib was similar (initial block size, $485 \times 172 \times 30 \text{ mm}^3$), but the order and clamping strategy deviated slightly (see Fig. 1c):

- Step 1: Face milling of backside in side clamps (feed per tooth $f_z = 0.2 \text{ mm}$, cutting speed $v_c = 730 \text{ m/min}$, radial cut depth $a_e = 40 \text{ mm}$, axial cut depth $a_p = 1.5 \text{ mm}$)
- Step 2: Side milling in side clamps ($f_z = 0.055 \text{ mm}$, $v_c = 450 \text{ m/min}$, $a_e = 2.5 / 0.5 \text{ mm}$, $a_p = 4.4 / 22 \text{ mm}$)
- Step 3: Drilling holes in side clamps
- Step 4: Face milling of top in side clamps and screws ($f_z = 0.2 \text{ mm}$, $v_c = 730 \text{ m/min}$, $a_e = 40 \text{ mm}$, $a_p = 1.5 \text{ mm}$)
- Step 5: Milling of pockets in side clamps and screws ($f_z = 0.2 \text{ mm}$, $v_c = 200 \text{ m/min}$, $a_e = 4 \text{ mm}$, $a_p = 3 \text{ mm}$)

A cutter with indexable inserts (Sandvik¹ R590-110504H-NL H10) was used to face mill the top and backside surface (step 1, 4) and a regular end mill (Kennametal¹ F3AA1200AWL) to side mill the walls (step 2) and pockets (step 5). MIRS from the cutting operations face milling (step 1, 4) and pocket milling (step 5) were measured in the previous research and plotted in Fig. 2. For more information we refer to [17–20]. Since the total machined part is 20 mm thick, different z-offsets of the part in the 30 mm stock are possible: a symmetrical position, removing 5 mm each at top and bottom, and an asymmetrical one, removing 1.5 mm at the bottom and 7.5 mm at the top were investigated. To achieve high feed rates, the pockets were milled in multiple layers with constant cutting parameters. The milling path strategy was varied from part to part from zig (machining in horizontal lines) to spiral path (machining from the inside out in spirals following the contour of the pockets). To prevent the distortion of the parts during pocket machining, the parts were held down by screws in addition to the clamping with side clamps. The backside surface was measured after the part was released from its clamping after step 5 with the coordinate measuring machine Tesa micro Hite 3D DCC¹ (repeatability limit ISO MPE-p 3.5 μm) to determine the distortion – here defined as the out of plane displacement in z-direction – caused by the RS. For the feature sample (wing rib), a spacing of the measured points of 2 mm (4 mm) with a distance to the edge of 1 mm (2 mm) was chosen, which resulted in 4714 (4419) measurement points in total. The final part distortion was analyzed by first leveling the data

¹ Naming of specific manufacturers is done solely for the sake of completeness and does not necessarily imply an endorsement of the named companies nor that the products are necessarily the best for the purpose.

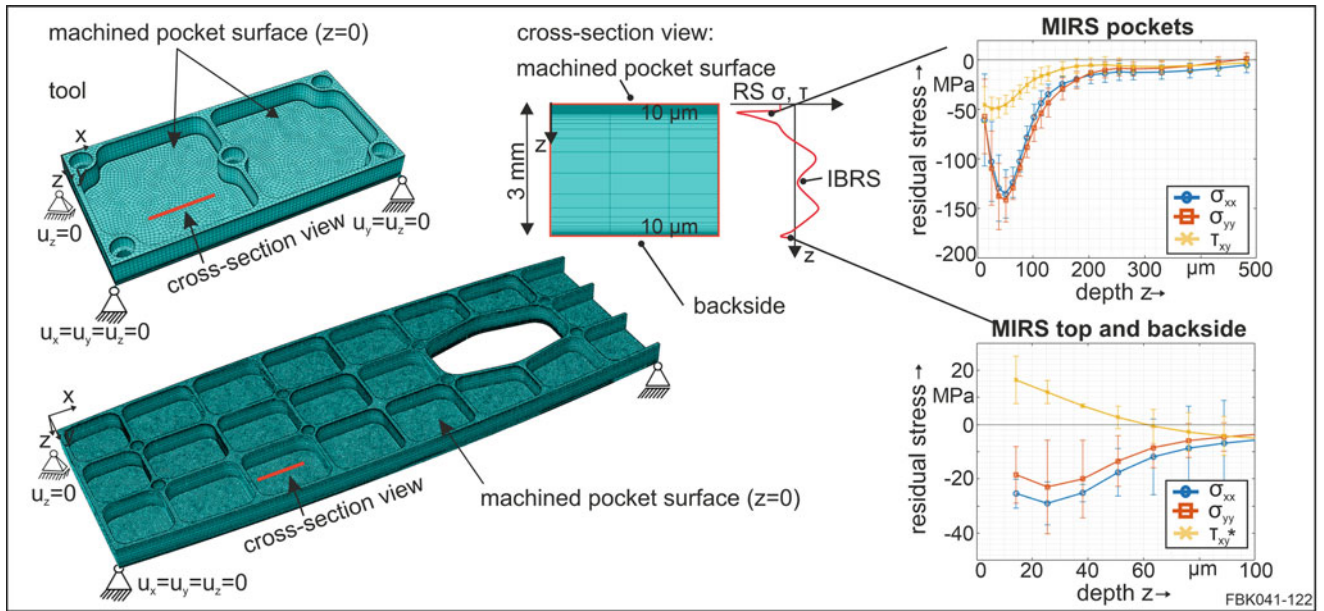


Fig. 2 FEM distortion model for feature sample and wing rib with MIRS from [23]

set (fitting a flat plane and subtracting it) and then setting a zero height at the resulting minimum, which was determined by averaging of the 10 (5) lowest measured points.

FEM Distortion Model

The developed FEM distortion model was presented and validated in previous research [17–20] and is now used to investigate the effect of varying IBRS on distortion for different part geometries. It is summarized here as follows: a static, linear elastic FEM model was set up in ABAQUS¹ ($E = 71,700$ MPa, $\nu = 0.33$). The measured MIRS and IBRS were implemented as an initial condition (type = stress) to the final part shape without modelling the material removal process. The MIRS were limited to a near surface layer (pocket floor, 200 μm ; backside/top, 70 μm ; see Fig. 3). IBRS were applied to the rest of the bulk. All RS $\sigma(z)$ were linearly interpolated over depth z at the element centroids. For the spiral milling strategy, a coordinate transformation of the MIRS according to the direction of milling was achieved (for more information see [20]). Previous research showed that MIRS in the walls have neglectable impact on the distortion in z -direction [20] and were therefore not considered in the distortion model. The mesh of the feature sample (wing rib) consisted of 670,308 (2,096,508) eight-node brick (C3D8) elements. The global mesh size was 1.5 mm and was refined in the near surface layer down to 10 μm to resolve the MIRS properly. The parts were minimally constrained (3-2-1 constraint principle [15]) to avoid rigid body motion but to enable a free part distortion (see Fig. 2). After one simulation step (reaching RS equilibrium), the displacement at the parts backside was analyzed according to experiments (leveling and shifting data) and compared to the measured distortion.

Results

The results section is divided into two parts: the IBRS results and the distortion results including measurements and simulations.

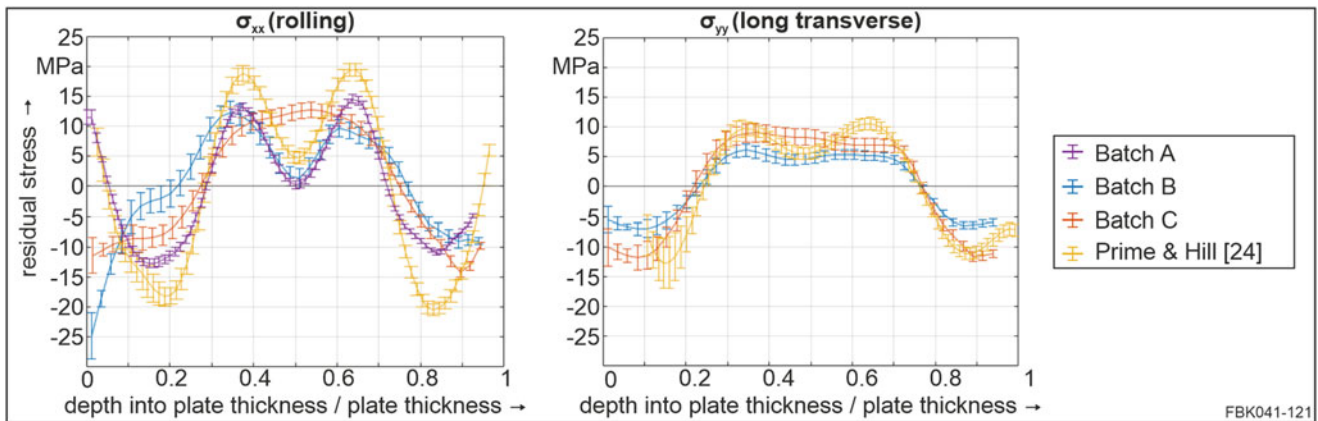


Fig. 3 Initial bulk residual stress comparison of measured and literature values of AA7050-T7451

Initial Bulk Residual Stress Measurements

Figure 3 depicts the measured IBRS and literature values from Prime and Hill [24] in x - and y -direction over the beam thickness normalized by the plate thickness. Most RS depth profiles showed the typical M shape of stresses with compressive RS close to the surface and tensile RS in the center. Batch C showed a \cap shape rather than an M shape, which could be due to the distribution of strength through the thickness of the corresponding plate (see [24]). The peak magnitudes of IBRS in the three batches were similar, being 10–15 MPa, with stress magnitudes slightly larger along the rolling (x) direction than along the long transverse (y). The stress magnitudes in the present samples are smaller than those from the literature, which reached peak levels of 20 MPa. The trend in σ_{xx} for batch B at depths less than 20% of the plate thickness reflects outlying behavior, the cause for which is unclear. Overall, the results show residual stress with a clear, symmetric M shape in batch A, a less clear and less symmetric M shape in batch B, and a \cap shape in batch C. The results are reasonably consistent with the prior work [24], which found similar trends in two plate thicknesses (80 mm and 25 mm), the thicker plate having a more distinct M shape.

Distortion

Figure 4 depicts the color maps of the measured distortion of the feature samples with different machining paths and z -offsets, as well as their simulated counterparts with different IBRS used as input. The orientation of the color maps is top view, meaning looking down to the milled pocket surface with positive distortion into the surface in positive z -direction. First the measurements are discussed before comparing simulated and measured distortions.

A slightly twisted distortion with the minima at the bottom left and top right corner and their maxima close to the top left and bottom right corner ($z_{\max} = 0.211$ mm) was evident for the feature sample milled with zig milling strategy (see Fig. 4a). The shear MIRS induced a torsional moment in addition to the bending moment of the IBRS and the normal compressive MIRS [17–20, 23]. Changing the milling direction also resulted in a change of the distortion shape: a U shape with the maximum distortion in the middle of the part's length ($x = 100$ mm) and regions where the tool cut first in the material (highlighted with black arrows in Fig. 4) was evident ($z_{\max} = 0.134$ mm). Due to the change of direction of the milling path to a spiral path, the distortion was reduced compared to the zig milling path, because the sign of the shear MIRS changed in 90° rotated regions. This led to an equilibration of the shear MIRS [20] and to a shift of the RS type dominating from MIRS to IBRS [23]. Choosing a z -offset of 5 mm of the final part in the raw material (Fig. 4c) instead of 1.5 mm decreased the distortion ($z_{\max} = 0.104$ mm), because the IBRS were then symmetrically distributed over the height z , inducing therefore a smaller bending moment [23].

The shape, including the position of the maximum distortion, was predicted correctly by all simulations using different IBRS inputs – except for regions where the tool ramped in for the spiral milling path (highlighted with black arrows in Fig. 4). This could be attributed to the presence of deviating MIRS in those regions due to different machining kinematics. Surprisingly, the level of distortion varied significantly when using different IBRS as input for all investigated cases, although IBRS magnitude varied only by about 5 MPa. The distortion level was predicted best with the simulations using the IBRS

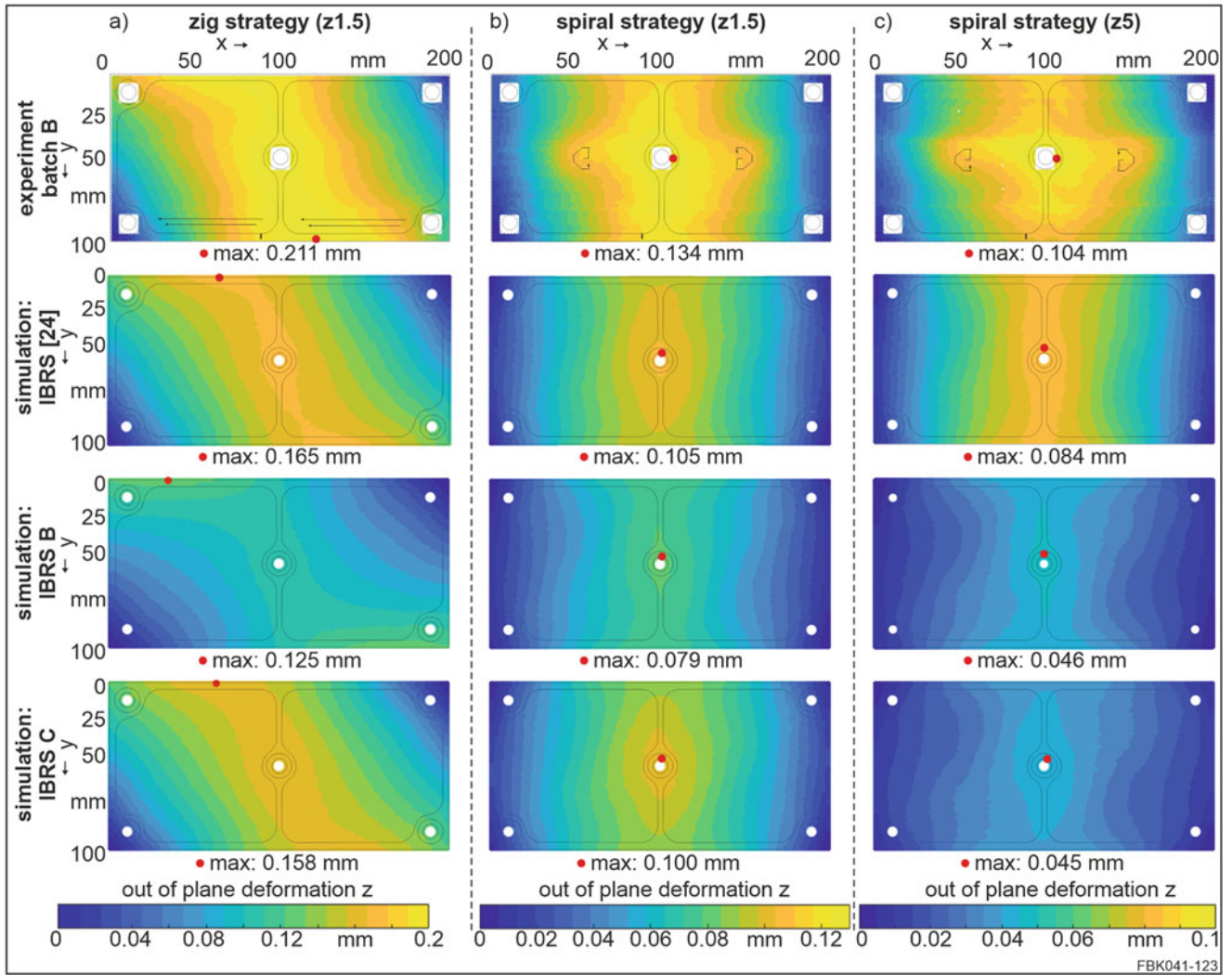


Fig. 4 Color maps of the measured and simulated distortions of the feature sample for different milling paths, z-positions and IBRS: zig strategy z1.5 (a), spiral strategy z1.5 (b) and spiral strategy z5 (c)

literature values from Prime and Hill [24] instead of the measurements done on samples from the same batch B material. Deviations (in terms of differences between prediction and measurement) of the maximum distortion down to 22% (Fig. 4a; zig – z1.5), 21% (Fig. 5b; spiral – z1.5), and 19% (Fig. 4c; spiral – z5) were found. All trends discussed for the measured distortions were matched by the simulations.

Figure 5 highlights the color maps of the measured distortion of the wing rib with different machining paths, as well as their simulated counterparts with different IBRS used as input. For the distortion measurements, the same trends as discussed for the smaller feature sample were found: a twisted distortion shape for zig milling ($z_{\max} = 0.739$ mm) and a U-shaped reduced distortion for spiral milling ($z_{\max} = 0.676$ mm) were evident.

The wing rib shape was predicted correctly by all simulations using different IBRS inputs. Small deviations for the position of the maximum distortion for zig milling strategy were found. This could be attributed to the fact that in experiments outer machining paths were not perfectly horizontal as assumed in the simulation, due to the curved shape of the part. Again, the highest accuracy of the simulation was reached when using the IBRS from the literature as input. Deviations down to 7% (Fig. 5a; zig – z5) and 28% (Fig. 5b; spiral – z5) were achieved. Using the measured IBRS led to an underestimation of the distortion for both investigated cases. One possible explanation for this trend could be that the IBRS in the beam specimens deviate from the IBRS in the remainder of the plate stock (which is perhaps closer to the literature values); this could occur if the beams were closer to the edges of the original plate stock, but this remains unknown.

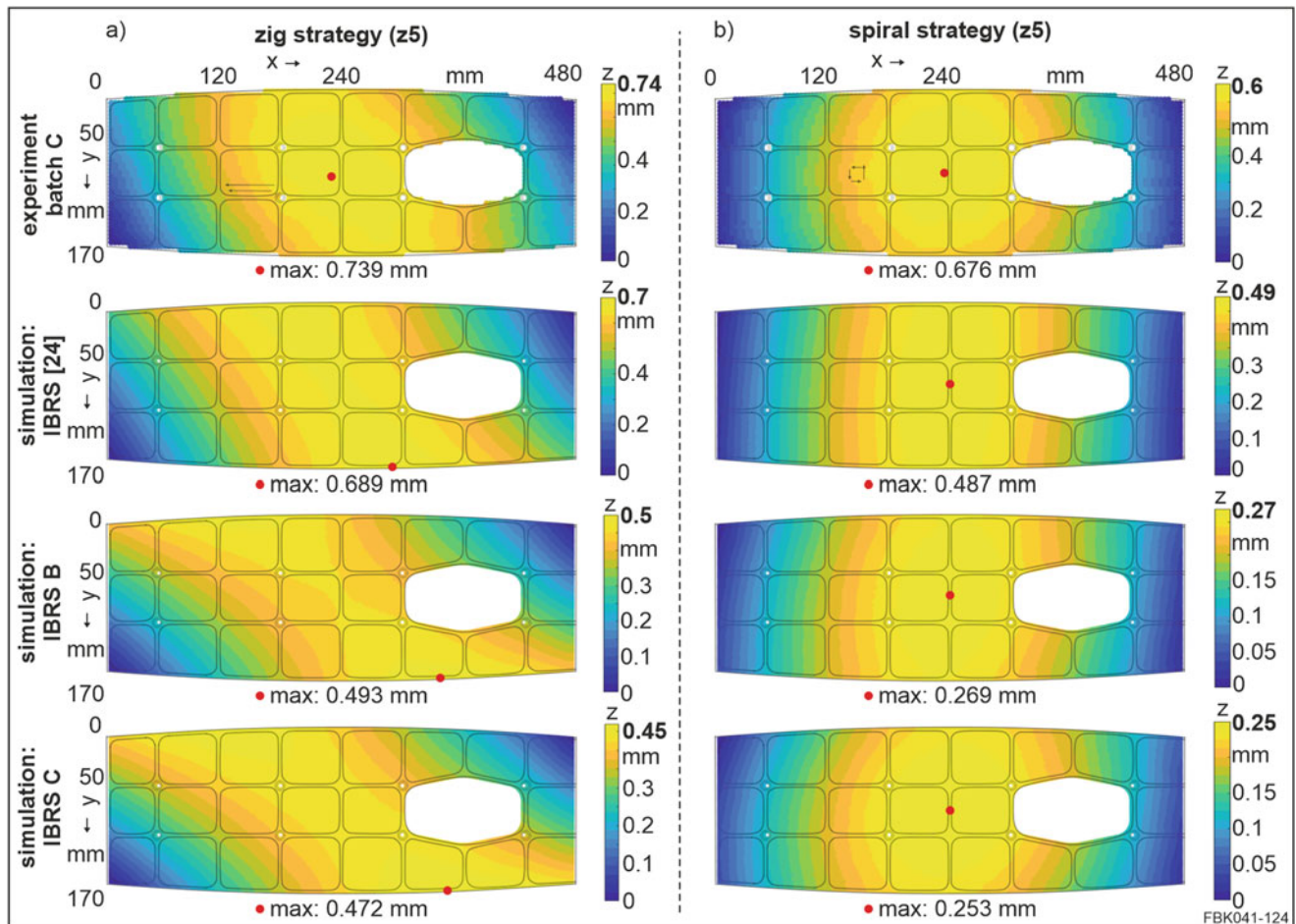


Fig. 5 Color maps of the measured and simulated distortions of the wing rib for different milling paths and IBRS: zig strategy z5 (a) and spiral strategy z5 (b)

Conclusion

IBRS measurements of different batches of A7050-T7451 are reasonably consistent with what was found in the literature by Prime and Hill [24] with a clear, symmetric M shape in batch A, a less clear and less symmetric M shape in batch B, and a \cap shape in batch C. The magnitude of the measured IBRS was slightly smaller than literature values (by about ~ 5 MPa). When using the different IBRS as input for the FEM distortion model in addition to the MIRS, the shape of distortion was predicted correctly for different geometries and milling strategies and for different z-offsets. However, the level of distortion, identified by the maximum, was underestimated when using the measured IBRS as input. The best results were achieved when using the IBRS literature values as input, in which case deviations of the maximum distortion of 28% (spiral-strategy) and 7% (zig-strategy) were evident.

Acknowledgments The authors would like to thank the German Research Foundation (DFG, Germany) and the National Science Foundation (NSF, USA) for the financial support within the project AU 185/64-1 (351381681) "NSF DFG Collaboration to Understand the Prime Factors Driving Distortion in Milled Aluminum Workpieces" (NSF funding Award No. 1663341) and within the International Research Training Group 2057 – Physical Modeling for Virtual Manufacturing (IRTG2057), Funding No. 252408385. Any opinions, findings, and conclusions or recommendations expressed in this material are those of the authors and do not necessarily reflect the views of the NSF or DFG.

References

1. Klocke, F.: *Fertigungsverfahren 1 – Zerspanung mit geometrisch bestimmter Schneide*. Springer Vieweg, Berlin (2018)
2. Jayanti, S., Ren, D., Erickson, E., Usui, S., Marusich, T., Marusich, K., Elanvogan, H.: Predictive modeling for tool deflection and part distortion of large machined components. In: *Procedia CIRP 12 – Proceedings of the 8th CIRP Conference on Intelligent Computation in Manuf. Eng.*, pp. 37–42, Naples (2013)
3. Berky, E.: *Aerostructures made in Augsburg*. In: *International ARO Seminar Aluminium-HSC Machining, Reutte (A)* (2001)
4. Li, J.G., Wang, S.Q.: Distortion caused by residual stresses in machining aeronautical aluminum alloy parts: recent advances. *Int. J. Adv. Manuf. Technol.* **89**, 997–1012 (2016)
5. Denkena, B., Boehnke, D., de Leon, L.: Machining induced residual stress in structural aluminum parts. *Prod. Eng.* **2**, 247–253 (2008)
6. Perez, I., Madariaga, A., Cuesta, M., Gray, A., Arrazola, P.J., Ruiz, J.J., Rubio, F.J., Sanchez, R.: Effect of cutting speed on the surface integrity of face milled 7050-T7451 aluminium workpieces. In: *Procedia CIRP 71 – Proceedings to the 4th CIRP Conference on Surface Integrity*, pp. 460–465. Elsevier BV (2018)
7. Rao, B., Shin, Y.C.: Analysis on high-speed face-milling of 7075-T6 aluminum using carbide and diamond cutters. *Int. J. Mach. Tools Manuf.* **41**(12), 1763–1781 (2001)
8. Tang, Z.T., Liu, Z.Q., Wan, Y., Ai, X.: Study on residual stresses in milling aluminium alloy 7050-T7451. In: Yan, X.-T., Jiang, C., B. (eds.) *Advanced Design and Manufacture to Gain Competitive Edge: New Manufacturing Techniques and Their Role in Improving Enterprise Performance*, pp. 169–178. Springer, London (2008)
9. Brooks, C.R.: Principles of heat treating of nonferrous alloys: heat treating of aluminum alloys. In: *ASM Handbook 4 Heat Treating*, pp. 1861–1960. ASM International (1991)
10. Keleshian, N., Kyser, R., Rodriguez, J.: On the distortion and warpage of 7249 aluminum alloy after quenching and machining. *J. Mater. Eng. Perform.* **20**, 1230–1234 (2011)
11. Chantzis, D., Van-der-Veen, S., Zettler, J., Sim, W.M.: An industrial workflow to minimise part distortion for machining of large monolithic components in aerospace industry. In: *Procedia CIRP 8 – Proceedings of 14th CIRP Conference on Modeling of Machining Operations*, pp. 281–286. Elsevier (2013)
12. Zhang, Z., Li, L., Yang, Y., He, N., Zhao, W.: Machining distortion minimization for the manufacturing of aeronautical structure. *Int. J. Adv. Manuf. Technol.* **73**(9), 1765–1773 (2014)
13. Cerutti, X., Mocellin, K.: Influence of the machining sequence on the residual stress redistribution and machining quality: analysis and improvement using numerical simulations. *Int. J. Adv. Manuf. Technol.* **83**, 489–503 (2016)
14. Dreier, S.: *Simulation des eigenspannungsbedingten Bauteilverzugs*, Dissertation, Hannover (2018)
15. Huang, X.M., Sun, J., Li, J.F.: Finite element simulation and experimental investigation on residual stress-related monolithic component deformation. *Int. J. Adv. Manuf. Technol.* **77**, 1035–1041 (2015)
16. Madariaga, A., Perez, I., Arrazola, P.J., Sanchez, R., Ruiz, J.J., Rubio, F.J.: Reduction of distortions in large aluminum parts by controlling machining-induced residual stresses. *Int. J. Adv. Manuf. Technol.* **97**, 967–978 (2018)
17. Weber, D., Kirsch, B., Chighizola, C.R., D’Elia, C.R., Linke, B.S., Hill, M.R., Aurich, J.C.: Analysis of machining induced residual stresses of milled aluminum workpieces, their repeatability and their resulting distortion. *Int. J. Adv. Manuf. Technol.* **115**, 1089–1110 (2021)
18. Chighizola, C.R., D’Elia, C.R., Weber, D., Kirsch, B., Aurich, J.C., Linke, B.S., Hill, M.R.: Intermethod comparison and evaluation of near surface residual stress in milled aluminum. *Exp. Mech.* **61**, 1309–1322 (2021)
19. Weber, D., Kirsch, B., Chighizola, C.R., D’Elia, C.R., Linke, B.S., Hill, M.R., Aurich, J.C.: Investigation on the scale effects of initial bulk and machining induced residual stresses of thin walled milled monolithic aluminum workpieces on part distortions: experiments and finite element prediction model. In: *Procedia CIRP 102 – Proceedings of the 18th CIRP Conf. on Modeling of Machining Operations*, pp. 337–342. Elsevier (2021)
20. Weber, D., Kirsch, B., Jonsson, J.E., D’Elia, C.R., Linke, B.S., Hill, M.R., Aurich, J.C.: Simulation based compensation techniques to minimize distortion of thin-walled monolithic aluminum parts due to residual stresses. *CIRP J. Manuf. Sci. Technol.* **38**, 427–441 (2022)
21. Hill, M.R.: The slitting method. In: Schajer, G.S. (ed.) *Practical Residual Stress Measurement Methods*. Wiley, West Sussex (2013)
22. Chighizola, C.R., Hill, M.R.: Two-dimensional mapping of bulk residual stress using cut mouth opening displacement. *Exp. Mech.* **62**, 75–86 (2022)
23. Weber, D., Kirsch, B., D’Elia, C.R., Jonsson, J.E., Linke, B.S., Hill, M.R., Aurich, J.C.: Simulation based investigation on the effect of the topology and size of milled thin-walled monolithic aluminum parts on the distortion due to residual stresses. In: *Proceedings of the International Conference on Residual Stresses (ICRS) 11, Archive ouverte HAL hal-03869964*, Nancy (2022)
24. Prime, M.B., Hill, M.R.: Residual stress, stress relief, and inhomogeneity in aluminum plate. *Scr. Mater.* **46**(1), 77–82 (2002)